

# ULRR

## Review of liquid-filled optical fibre-based temperature sensing

Item Type	Book chapter
Authors	McGuinness, Fintan;Leen, Gabriel;Lewis, Elfed;Dooly, Gerard;Toal, Daniel;Duraibabu, Dinesh Babu
Citation	Application of Optical Fibre for Sensing;2018
Publisher	Intech
Download date	2026-06-16 19:19:58
Item License	<a href="https://creativecommons.org/licenses/by-nc-sa/1.0/">https://creativecommons.org/licenses/by-nc-sa/1.0/</a>
Link to Item	<a href="https://hdl.handle.net/10344/7371">https://hdl.handle.net/10344/7371</a>

# Review of Liquid-Filled Optical Fibre-Based Temperature Sensing

*Fintan McGuinness, Gabriel Leen, Elfed Lewis, Gerard Dooly, Daniel Toal and Dinesh Babu Duraibabu*

## Abstract

While ever higher resolution temperature sensing is of demand in research and industry, the cost of sensors in the sub-milli-Kelvin (mK) range can be restrictive. Furthermore, as the majority of commercial temperature sensor measurements are transmitted via electrical circuits, significant post-processing is required to obtain a high-resolution due to phenomena such as electromagnetic interference, self-heating, electrical noise, etc. Consequentially, research in recent years has focused on the development of several technologies which overcome this issue, with optical fibre sensors proving to be a viable option. Owing to this, the following chapter will aim to review the current state-of-the-art in liquid filled optical fibre temperature sensing and the underlying methods.

**Keywords:** optical, fibre, temperature, sensor, liquid, review

## 1. Introduction

Prior to the development of thermometers, or indeed a scale of temperature, Renaissance Italy had already begun to question the nature of relative temperatures with scientific postulations such as *Bardi's problem*. This problem was posed by Count Bardi di Vernio to Galileo to determine why a person felt cold upon entering a river in summer, yet grew comfortable over time. While forgoing a direct solution to Bardi's Problem, Galileo reportedly developed a thermoscope in response [1]. Although the device was capable of showing variation in sensible heat it differed from a thermometer in that it did not have a defined scale, it also suffered from barometric influences due to the nature of its construction [2]. It should be noted at this point that there remains uncertainty over the original inventor of the thermoscope, however four prime candidates have been identified, these being; Galileo, Sanctorius Sanctorius, Robert Fludd and Cornelius Drebbel [1]. The advent of precision thermometry originated with the designs of Fahrenheit in the early eighteenth century, with his sealed mercury-in-glass thermometers being a significant advancement on the then state-of-the-art [2]. While specialised liquid-in-glass thermometers have demonstrated resolutions in the region of 0.2 K [3] they are the least useful for accurate measurements in a temporal sense. This is primarily due to the inability to perform transient measurements and relatively cumbersome geometry when compared to electronic sensors.

Currently, industrial temperature sensor designs typically rely on either the thermoelectric effect or temperature dependant resistance. Owing to their wide

operating range, thermocouples have been utilised in general engineering applications ranging from precision temperature control for tea processing factories to monitoring the cell temperatures of hepatoblastomas, with peak sensitivities in the region of 20 mK [4, 5]. However due to relatively poor response times, thermocouples are unsuited to high speed measurement. Another robust temperature sensor design is the negative temperature coefficient thermistor (NTC). A particular benefit to using NTCs is the ability to custom mould them for a desired application along with easily tunable resistance at the device and circuit levels [6]. Clow et al. [7] presented an array of NTCs used as a single sensor which was capable of 0.1 mK resolution with application in paleothermometry. While the sensor had excellent resolution it suffered from several drawbacks, the most relevant being a 7 s response time, which prevented it from recording highly transient temperatures gradients. Furthermore the sensor was sensitive to triboelectric effects from snow deposits on sensing wires and self-heating related noise, these being issues which scaled with distance. Precision resistance temperature detectors (RTDs) with milli-Kelvin (mK) resolution are readily available with a response time of 950 ms, and high-speed RTDs in the region of 400 ms [8]. While these sensors present high precision over their working range, a drawback of using RTDs is their inherent fragility. While suited for use in a laboratory, and other controlled environments, general deployment is still proving difficult at present. Hewlett & Packard pioneered the initial development of quartz thermometers in the mid-1960s, with resolution being in the range of 0.1 mK [9]. While capable of achieving sensitivity equivalent to the sensor presented by Clow et al. [7] the reported response time was 30% slower, and had a larger overall footprint.

The issues posed by the use of these *traditional* sensors in the presence of electromagnetic interference (EMI) and other considerations such as damage resilience and projected lifespan, has resulted in significant investment being made in the exploration of optical fibres as a means of high resolution temperature sensing. While still relatively fragile compared to thermocouples and glass bulb thermometers, optical fibre temperature sensors (OFTS) offer the possibility of a cost effective, high speed and precise sensor. The purpose of this review is to present the current state-of-the-art in a subset of optical fibre sensors that is to say, liquid-filled optical fibre temperature sensors (LiF-OFTS). Further to this, applications in which they have been utilised will be presented along with a discussion of potential future developments.

### **1.1 Temperature sensor requirements**

As temperature sensors can be a mission critical piece of equipment various standards have been issued with respect to their usage. Common publishers of temperature sensor requirements for calibration and reporting include the ASTM [10] and IEEE [11]. The measurement range of a given sensor is largely determined by the nature of its operating environment. In an industrial process the range may be several hundred Kelvin, whereas a homeostatic biomedical thermometer requires a range in the order of only 15 K [12]. Some commercially available probes made from exotic materials such as a tungsten-rhenium alloy thermocouples (Types G, C and D) have wide working ranges, approximately 273–2590 K [13]. These commonly find application in processes involving high temperatures, however require further protection if being utilised in an oxidising environment.

The overall resolution of a temperature sensor may be more important than the operating range depending on an intended application. While it is not critical that a domestic oven have precision temperature control, it can be of great assistance to

Company	General Electric	Hanna Instruments	SENSTECH
Sensor type	PRT [18]	TC (K-Type) [8, 19]	NTC [20]
Min. temperature	283 K	73 K	218 K
Max. temperature	450 K	573 K	398 K
Resolution	0.003 K	0.1 K	0.044 K
Response time	0.5 s	4 s	0.75 s
Accuracy	0.5 K	0.5 K	0.5 K

**Table 1.**  
 Commercially available high resolution temperature sensors.

pharmaceutical calorimetry. A review of the topic conducted by Buckton et al. [14] highlighted the need for identical and constant temperatures within the fermenter and calorimeter, along with maintaining an isothermal condition within the calorimeter itself. As the heat released in these reactions is typically of the order  $1 \times 10^{-4}$  mW it is readily evident that precision thermometry is beneficial in obtaining repeatable results. Rossi et al. [15] examined the relationship between intracranial and core temperatures in patients within 2–168 h post severe head injury. From this, intracranial temperatures were verified by comparison to the Delta OHM HD 9215, which had a resolution of 0.1 K. It was reported that core temperature was a poor indicator of intracranial temperature during pyrexia episodes, which was indicative of benefits to independent high resolution temperature sensing within the cranium. As magnetic resonance imaging (MRI) is common in patients post trauma, significant benefit would be provided should the thermometer be unaffected by the strong magnetic field, as it may remain in place to continue real-time monitoring.

Sampling rate is an important factor when deciding on a temperature sensor as it has to be considered in conjunction with the sensor response time. If the heat transfer from the system is known, then a rate of temperature change may be determined by Eq. (1) [16]. Evidently as temporal resolution is increased smaller variations in heat, and as a consequence temperature, may be determined.

$$\frac{\delta Q}{\delta t} = c \cdot \frac{\delta T}{\delta t} \quad (1)$$

Further to the items outlined above, specialised considerations may be required. In automotive engine development it is commonplace to embed multiple sensors inside the cylinder head/wall. While electronic sensors operate with little issue for the majority of a four-stroke cycle ( $720^\circ$ ) the spark plug activates for several degrees before or after top dead centre. As this is a period of strong pressure and thermal gradients, EMI introduced by the spark plug creates difficulty in analysing the recorded data [17]. A small sample of commercially available high resolution temperature sensors is presented in **Table 1**.

## 2. Advantages of optical fibre sensors

As mentioned in the introduction, optical fibre sensors present many advantages over their electronic counterparts. Therefore, the following section will examine several properties of optical fibres which indicate their viability as an alternative to electronic sensors.

## **2.1 Construction**

Commercially available silica fibres are widely used in the development of optical fibre temperature sensors owing to their small cross-sectional area and consequently their ability to be implemented in restricted areas. However, the relatively low cost of silica fibre compared to more exotic fibres such as those manufactured from fluoride or synthetic sapphire may be a factor to consider. As is reported, optical fibre sensors are particularly suited to environments where an electronic sensor may not have sufficient protection from EMI, and where line of sight to the measurement point is obstructed [21]. Furthermore, optical fibre sensors do not represent a potential source of ignition in an explosive environment; can be biocompatible; and can be made to work over very long distances. To date, optical fibre temperature sensors have been implemented in applications ranging from *in-vivo* biomedical sensing [22], to structural and geothermal engineering [23].

## **2.2 Measurement stability**

In civil engineering applications, such as bridges, use of chirped fibre Bragg gratings (FBGs) provide excellent through life performance as fibre degradation is in excess of 25 years [24] with data transmission losses being minimal [23]. Furthermore, stability of measurements are generally quite good due to performance being driven predominantly by the wavelength stability of light source used. This being an easy factor to account for, as said light source may be kept in a controlled environment.

## **2.3 Distributed sensing**

In addition to the EMI resistance and dimensional advantages of using optical fibre sensors, their ability to provide multipoint sensing with minimal use of fibre is a desirable characteristic. One such method is the use of chirped FBGs whereby multiple FBGs are inscribed on a single fibre, with the grating period modified at each location thus providing high spatial resolution. Wave division multiplexing (WDM) is another commonly used method in multi-point sensing with optical fibres, however this method narrows the usable bandwidth of light proportionally to the number of fibres used. Historically, Raman scattering has been used as an efficient means of multi-point temperature measuring; however, Brillouin sensors reported have shown exceptional strain measurement capability for an equivalent temperature sensing performance [25].

## **3. Theory and working principles**

In the use of optical fibres for temperature sensing, measurements can be conducted using both intrinsic and extrinsic techniques. The most common technique for assessing temperature changes using optical fibres is the use of interferometry. Examples being fibre Bragg gratings (FBGs), extrinsic Fabry-Perot interferometers (EFPIs), Mach-Zehnder interferometers (MZIs) and Sagnac interferometers (SIs). As the fibre requires a light source to conduct the measurement, various types have been explored such as; broadband light source [26] monochrome laser [21] and swept laser [27]. Measurements can be carried out by observing either the transmitted spectrum, or the reflected spectrum. When recording the reflected spectrum losses occur in the back reflections through the fibre and at the coupler between the light source and spectrometer. That said however, this method allows

for the fibre to be used as a point measurement device in applications where transmission is impractical, i.e. biomedical [28], automotive [29], and pharmaceutical [30] sensing. As the modus operandi of any particular optical fibre sensor is modulation of the light source, this can be carried out via intensity, frequency, or phase modulation. The latter of which will be the main focus of the review as this is the method typically employed by LiF-OFTS.

### 3.1 Fibre Bragg gratings

Fibre Bragg gratings are created by periodically modifying the refractive index of an optical fibre core. At each change of refractive index the reflected light constructively interferes producing a high intensity narrowband signal. This effect is described by Eq. (2) where  $\lambda_B$  is the Bragg wavelength,  $n_{eff}$  is the effective refractive index, and  $\Lambda$  is the pitch between each of the modified refractive indices. **Figure 1** provides a schematic of an FBG inscribed on a fibre core. As is evident from Eq. (2) care must be taken to eliminate, or account for, mechanical straining of the fibre as this will artificially modify the grating period. Once mechanical strain has been determined the change in Bragg wavelength with temperature is given by Eq. (3). A review on the packaging of FBGs is provided by Hong et al. [31].

$$\lambda_B = 2n_{eff} \cdot \Lambda \quad (2)$$

$$\frac{d\lambda_B}{dT} = 2 \left( n_{eff} \cdot \frac{d\Lambda}{dT} + \Lambda \cdot \frac{dn_{eff}}{dT} \right) \quad (3)$$

Owing to the simple nature of their construction FBGs have been utilised to great success as a means of sensing temperature, however they are not without inherent issues such as damage due to exposure to excessive temperatures [22], and grating orientation to the heat source [32]. Zhang et al. [22] reported the assessment of cylinder head temperature and mixture flow within maritime diesel engines, where significant steps were taken to protect the fibre coating from excessive cylinder head temperatures (873.15 K). Gassino et al. [32] examined the use of FBGs in the presence of strong temperature gradients ( $\sim 10$  K/cm) during thermal ablation of tumours. Several key design factors were discussed from which it was determined the largest sources of error were caused by the temperature gradient along the length of the FBG, and FBG orientation with respect to the temperature gradient.

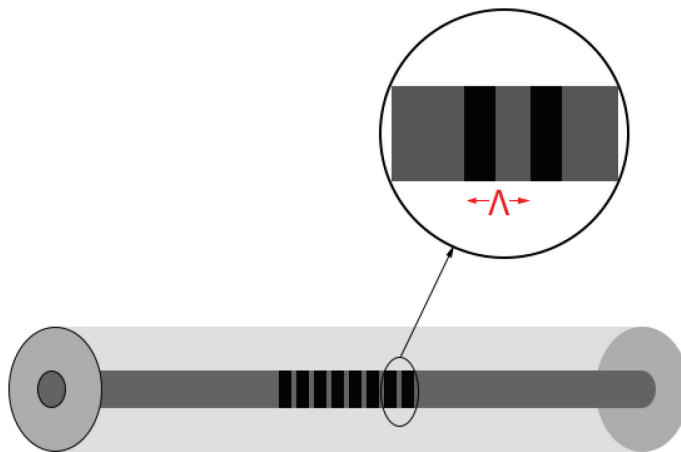


**Figure 1.** Schematic of FBG, highlighting grating pitch ( $\Lambda$ ) in fibre core.

### 3.2 Extrinsic Fabry-Perot interferometers

Fabry-Perot based sensors are typically extrinsic in nature and used as a point measurement device at the tip of an optical fibre. A common construction of EFPI sensors involves a single mode fibre (SMF) spliced to a capillary with a multi-mode fibre (MMF) which acts as a diaphragm fused to the opposing end of the capillary, creating an air filled cavity between the SMF and MMF. **Figure 2** highlights the dimensions relevant to diaphragm deflection and rigidity, with the construction presented in **Figure 3**. As light reaches the end face of the SMF a portion of the light is reflected, with the remainder transmitted into the air cavity. Similar reflections occur at the air-diaphragm, and diaphragm-external media interfaces. As the light reflected from the inner and outer faces of the diaphragm has travelled a greater distance, than the light reflected at the end face of the SMF, a phase difference between reflections will exist. While FPIs behave similar to FBGs in that they have varying refractive indices along the axial direction, adjustment of the diaphragm thickness can be used as a means of increasing pressure sensitivity by modifying the diaphragm flexural rigidity. Said flexural rigidity is determined by Eq. (4) [33] where  $h$ ,  $E$  and  $\nu$  are the diaphragm thickness, Young's modulus, and Poisson's ratio respectively. Eq. (5) [33] provides the relationship between diaphragm displacement and uniformly applied pressure, this being fundamental to the temperature sensor presented by Poeggel et al. [34]. From this it becomes apparent that a thinner diaphragm leads to greater maximum deflection, and said maximum deflection occurs at the diaphragm centre.

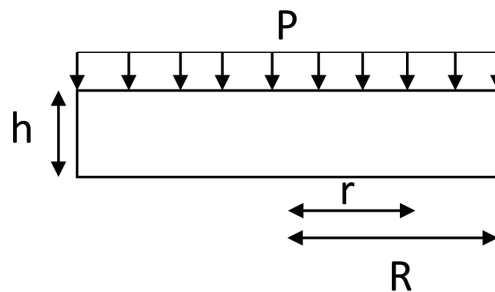


**Figure 2.**  
Dimensions which influence diaphragm flexural rigidity and deflection.

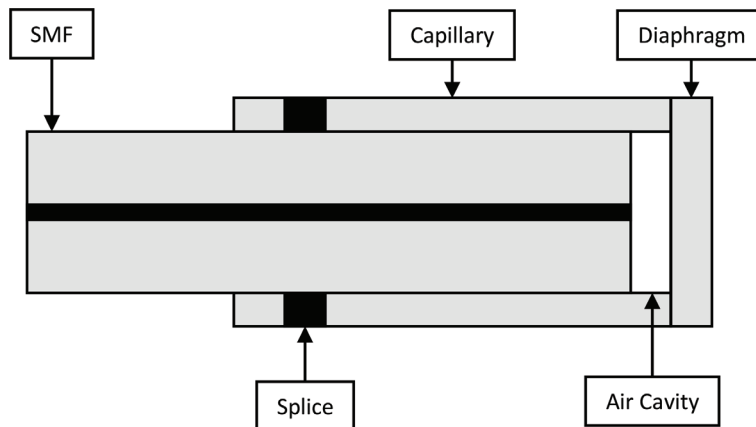


**Figure 3.**  
Schematic of typical EFPI.

$$D = \frac{Eh^3}{12(1 - \nu^2)} \quad (4)$$

$$z(r) = \frac{3}{16} \cdot \frac{(1 - \nu^2)(R^2 - r^2)}{Eh^3} \cdot P \quad (5)$$

Gao et al. proposed an alternative construction, using particle vapour deposition (PVD) to create a ‘diaphragm’, which was fused directly to an MMF [35]. This construction provides a number of advantages, such as a robust construction, and the ability to custom tune optical path lengths without the uncertainties related to splicing. Eq. (6) presents the relationship between the optical path differences (OPD) with the thermal coefficients of refractive index ( $\alpha_n$ ) and material thickness ( $\alpha_d$ ) for the PVD diaphragm.

$$\frac{OPD(T)}{OPD(T_0)} \approx 1 + (\alpha_n + \alpha_d)(T - T_0) \quad (6)$$

### 3.3 Mach-Zehnder interferometers

Mach-Zehnder interferometers (MZIs) operate by splitting the source light and introducing an optical path difference, before recombining the beams prior to the detector [36]. As a means of sensing in optical fibres, common practice has been to splice a length of photonic crystal fibre (PCF) between two lengths of SMF [37–40]. These operate by allowing the core mode of the SMF to be split into core and cladding modes at the first splice point within the PCF. These are subsequently rejoined at the second splice point with an interference between the two modes becoming apparent in the transmission, this is usually represented by resonant dip (s) in the signal transmitted to the optical spectrum analyser (OSA). Modification to the air holes of the PCF is commonly carried out via collapsing or filling with various fluids, in order to increase sensitivity to the desired measurand. For the purpose of temperature sensing it is common to fill the PCF holes with a fluid which has a high magnitude (as it may be positive or negative) thermo-optic coefficient [37, 39, 41, 42]. **Figure 4** below provides a schematic of how a typical MZI sensor setup is presented in literature. In a PCF the two branches of the MZI are the cladding and core modes respectively. A transverse section of a PCF is presented in **Figure 5** where the core, and cladding air holes are highlighted.

### 3.4 Sagnac interferometers

Sagnac interferometers (SIs) behave similarly to MZIs in that they compare optical path differences of two beams which have been split and subsequently recombined. However, they differ such as the two beams counter-propagate with

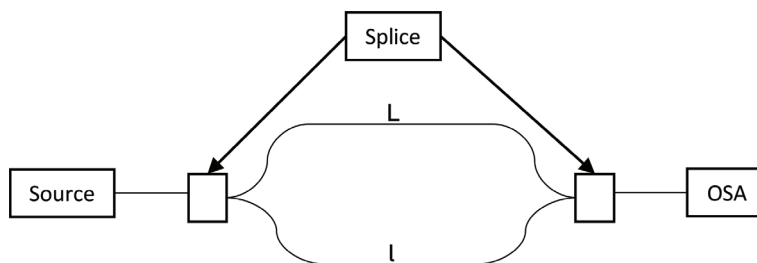


**Figure 4.**  
 Schematic of Mach-Zehnder based sensor.

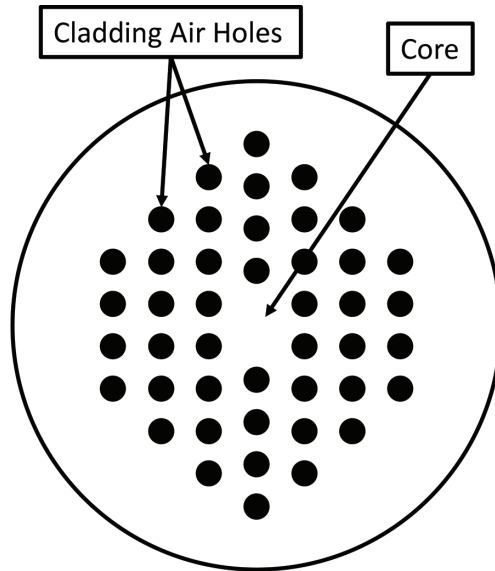


**Figure 5.**  
*Transverse section of a photonic crystal fibre.*

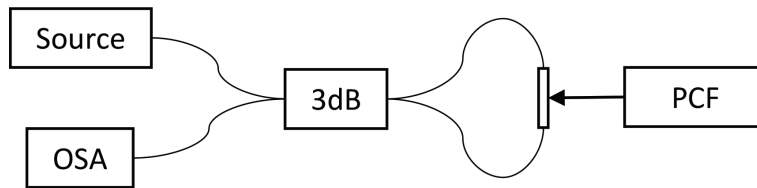


**Figure 6.**  
*Schematic of potential Sagnac interferometer based sensor.*

respect to each other before being recombined at the detector. This type of interferometer is the basis of fibre-optic gyroscopes [43]. While it has been utilised in thermometry [44, 45] the sensors reported have not seen a similar level of research compared to their MZI counterparts. Reported sensors used a source beam counter-propagated by a 3 coupler. Birefringence in the PCF resulted in the optical path difference which was detected by the OSA [44, 45]. **Figure 6** above highlights how an SI based sensor may be constructed using optical fibre equipment.

#### 4. Liquid filled optical fibre temperature sensors

As evident from Sections 1 and 3 temperature sensors have a long history. With respect to LiF-OFTSs however, while several types of sensor and base technologies have been presented in the literature, the authors have not encountered a concise review of said sensors. The materials utilised have included; alcohol [44] motor oil [34], silicone (polydimethylsiloxane) [46], and immersion oils [39]. While polydimethylsiloxane (PDMS) has only been presented in its cured form, it is not inconceivable that the liquid form be used given its optically transparent nature. The following section is arranged by the base interferometry principle of each fluid filled sensor.

#### 4.1 EFPI type sensors

Chen et al. presented an FPI construction which contained an air micro-bubble encased in cured PDMS [46]. The sensor was manufactured by splicing an SMF to a hollow core fibre (HCF) 282  $\mu\text{m}$  in length. The PDMS was subsequently introduced into the HCF via capillary effect. As PDMS entered the HCF it formed the air micro-bubble with the SMF, where the length of air micro-bubble was controlled by the period of time PDMS was allowed to enter the HCF. Online monitoring was conducted to establish the free spectral range (FSR) best suited to the desired application. A schematic of the sensor is presented in **Figure 7**.

The PDMS was cured for 45 min at 338.15 K, fixing the length of the air micro-bubble. Testing was conducted between 324.35–343.65 K and compared to a PT100 thermometer with a resolution of 0.01 K. Results indicated sensitivity was quite high with a value of 2.7035 nm/K and a highly linear response where  $R^2 = 0.992$ . In addition to the reported sensitivity, reference was made to the benefit of using a double FPI in the sensor. This consisted of a thin FPI (air micro-bubble) and thick FPI (PDMS filling). The thin FPI allowed for a large FSR and the thick FPI offered high temperature resolution.

Poeggel et al. [34] presented a novel ultra-high resolution temperature sensor (UHRTS). The sensor was comprised of an existing optical fibre pressure temperature sensor (OFPTS) [47] which was further encased in an outer oil-filled capillary. The sensor was noted to have an external diameter of less than 1 mm lending to its capability to be used in volume restricted areas, a schematic of the sensor is provided in **Figure 8**. By combining an FBG with the highly sensitive EFPI, the UHRTS behaved similar to that of Chen et al. [46] in that the FBG and air cavity allowed for a wide spectral range to be utilised with the diaphragm element providing high resolution. Dissimilar to Chen et al. however, the construction of the OFTS was reliant on the thin diaphragm element to transduce volume changes in the oil to a temperature measurement. This being demonstrated by Eqs. (4) and (5) in Section 3. It was claimed that the high ratio of oil in the outer capillary compared to air in the EFPI cavity was what resulted in high sensitivity. The sensor presented had a reported, theoretical, sensitivity of  $52.7 \times 10^3$  nm/K. Comparison of the UHRTS to a Bosch BMP085 [48] was carried out over a temperature range of 7 K. While both sensors detected the 7 K variation, measured EFPI sensitivity was much lower than predicted, at 8.77 nm/K. It was suggested that the error was likely caused by inconsistencies in the manufacturing process of the sensor, and the presence of micro air bubbles in the oil which resulted in response damping. Considering oil was introduced into the capillary via a micro-syringe rather than by capillary effect as utilised by several authors such as Chen et al. [46] and Xu et al. [39] this may have

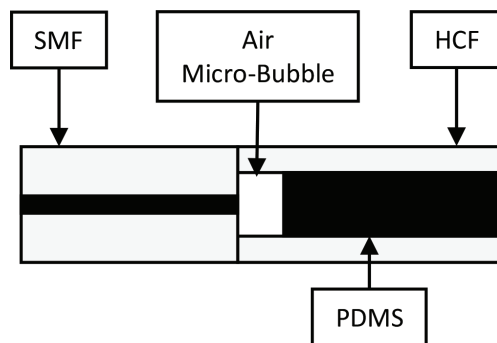


**Figure 7.**  
Schematic of PDMS FPI sensor based on Chen et al. [46].

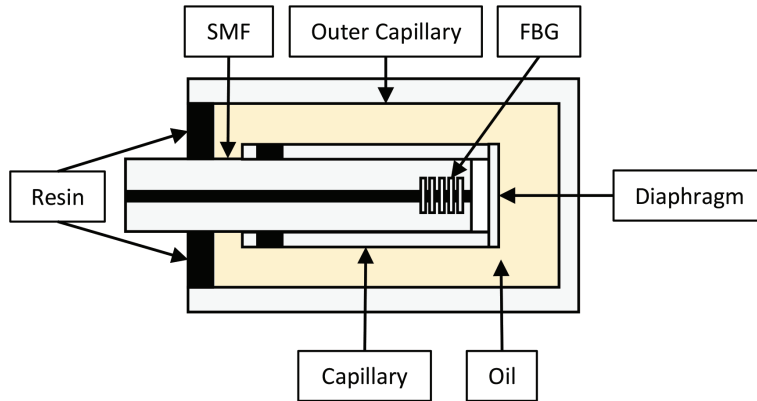


**Figure 8.** Schematic of oil-filled EFPI sensor based on Poeggel et al. [34].

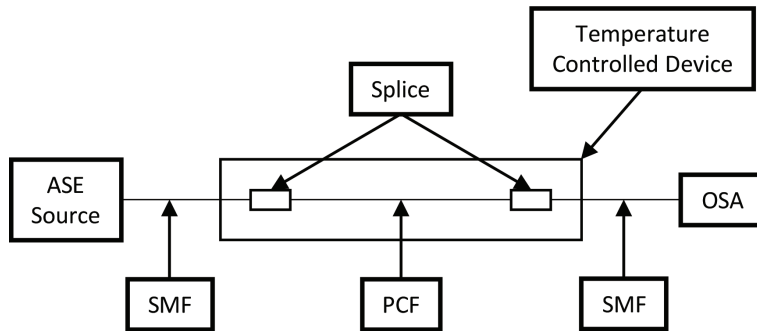


**Figure 9.** Schematic of an inline PCF sensor based on Qiu et al. [37].

been a contributing factor to bubble formation. Another potential application of the sensor proposed by Poeggel et al. [34] is use of an ionising radiation sensitive fluid whereby the temperature response varies with exposure to ionising radiation.

#### 4.2 Mach-Zehnder interferometer type sensors

Qiu et al. [37] presented a temperature sensor based on a non-polarimetric PCF, where the sensor was created by splicing a length of commercial single mode (LMA-8) [49] between two lengths of SMF-28. During construction, isopropanol was infused into the non-polarimetric PCF micro-holes by capillary effect, with the PCF subsequently fused between the SMFs. LMA-8 PCF was chosen due to having a diameter equal to that of the SMF-28, this reduced potential complications involved in the splicing process, care was also taken to minimise collapsing of the fibre air holes. Thermo-optic coefficients (TOCs) for the isopropanol and silica are  $-4.5 \times 10^{-4}/\text{K}$  and  $8.6 \times 10^{-6}/\text{K}$  respectively. A schematic for the sensor is provided in **Figure 9**, where an amplified spontaneous emission source (ASE) was used. As light entered from the SMF into the PCF, cladding and core modes propagated at different rates before recombining at the second splice point, this process introduced a phase difference which was observed to be temperature dependant. Akin to the designs of several other fluid-filled inline sensors, this sensor also relied on modifying the core and cladding mode TOCs in order to maximise temperature sensitivity. The sensor was tested in a temperature controlled device over temperatures ranging from 296.85–339.25 K. Blue-shifting of the two tracked waveform dips was

observed. A sample of how these waveforms may appear is presented in **Figure 10**. Temperature sensitivities were reported as  $-133$  and  $-166$  pm/K respectively. While this was an order of magnitude improvement over previously published works [50–52] it was significantly less sensitive when compared to the design of Qian et al. [44], indicating that exploiting the birefringent nature of PCFs may be highly beneficial in the development of inline PCF sensors.

Wang et al. [38] presented a fluid-filled PCF-based modal interferometer (PCFMI). The air holes of the PCF were filled with an oil provided by Cargille Laboratories Inc. (Cedar Grove, NJ, USA) ( $\text{TOC} = -3.37 \times 10^{-4}/\text{K}$ ). The system design was similar to that of Qiu et al. [37]. That said however, the operation has similarities to that of Wang et al. [41] with the interference of  $\text{LP}_{01}$  and  $\text{LP}_{11}$  modes at the second splicing (recombination) point. Simulation suggested that temperature sensitivity increased proportionally with the ratio of filled to unfilled PCF, and that for constant filling ratio the sensitivity increased with increasing wavelength. It was reported that the latter was due to larger mode field areas of the longer wavelengths. Validation experiments were carried out at three filling ratios ( $k = 0.256, 0.282, 0.476$ ) over a temperature range of 298.15–355.15 K. Results were in agreement with theoretical prediction, transmission spectra blue-shifted with increasing temperature, and the largest filling ratio ( $k = 0.476$ ) resulted in the highest temperature sensitivity. Similarly, longer wavelengths resulted in increased sensitivity with a peak value of  $-340$  pm/K at 1480 nm. Another benefit of the proposed sensor type is the linear response to straining, once matrix values were determined, the wavelength shifts may be used to produce temperature and strain measurements simultaneously. The matrix for the sensor presented by Wang et al. is provided by Eq. (7) where  $S_T$  and  $S_\varepsilon$  are the temperature and strain sensitivities respectively. A and B are the two waveform dips which were monitored.

$$\begin{bmatrix} \Delta T \\ \Delta \varepsilon \end{bmatrix} = \begin{bmatrix} S_{T,A} & S_{\varepsilon,A} \\ S_{T,B} & S_{\varepsilon,B} \end{bmatrix}^{-1} \begin{bmatrix} \Delta \lambda_A \\ \Delta \lambda_B \end{bmatrix} \quad (7)$$

Wang et al. [41] presented an ultra-high resolution PCF sensor which had a single liquid filled cladding hole. In the precision filling of the hole, an initial 10  $\mu\text{m}$  end cap was placed on the PCF, after which a hole was precision drilled into the desired PCF hole using a femtosecond laser (FSL). A Cargille Laboratories Inc. immersion oil with a  $\text{TOC}$  of  $-3.89 \times 10^{-4}$  was introduced via capillary effect. The filled region of PCF was subsequently reduced incrementally by  $\sim 1$  cm until a coherent resonant dip was present. Experimental results between 307.15 and 308.55 K indicated exceptional sensitivity at 54.3 nm/K. Linearity of the results was not provided. Numerical comparison was carried out in Comsol Multiphysics where

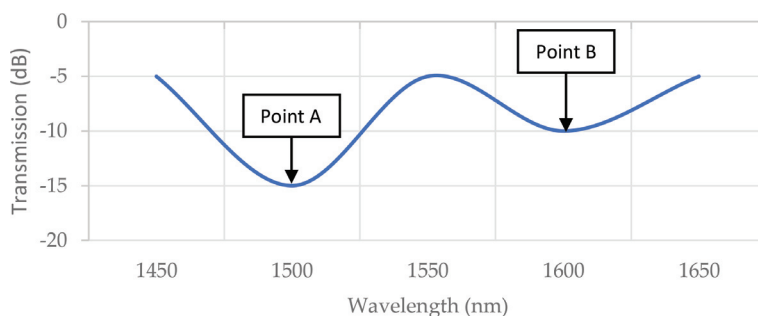


**Figure 10.**  
 Representation of how two waveform dips may appear in a transmission spectrum.

the fibre and liquid rod core modes were compared. Results indicated coupling only occurred between the respective  $LP_{01}$  modes, where the coupling wavelength shifted by 292 nm between 303.15 and 308.15 K this giving a projected sensitivity of 58.4 nm/K. While predicted sensitivity largely agreed with experimental observations, the location of the dip did not. It was determined that this was predominantly due to uncertainty surrounding the refractive index of the immersion oil, as it had a tolerance of  $\pm 0.002$ , where an error of 0.001 led to a 150 nm wavelength shift.

Liang et al. [42] reported the first double-filled PCF sensor, with the two fluid rods having varied optical properties, both immersion oils were provided by Cargille Laboratories Inc. The first had a refractive index (RI) of 1.466 with a TOC of  $-3.91 \times 10^{-4}$  and the second 1.500 with a TOC of  $-4.01 \times 10^{-4}$  respectively. Owing to energy differences the PCF  $LP_{11}$  core mode was neglected. Finite element analysis indicated an interaction existed between  $LP_{01}$ (core)– $LP_{01}$ (rod 1), and  $LP_{01}$ (core)– $LP_{11}$ (rod 2). This indicated two waveform dips would be present in the transmission spectrum. Furthermore rod 1 displayed red-shift with increasing temperature with the converse being true of rod 2. As the two liquid rods were relatively far apart geometrically, there was no reported interaction. Temperature response was recorded between 325.15 and 327.15 K in increments of 0.2 K. Dip sensitivities were recorded as being 42.818 and  $-11.343$  nm/K with linearities of  $R^2 = 0.99951$  and  $0.99935$ , thus indicating the sensor had extremely high sensitivity. A highly sensitive strain response was also reported. Force on the fibre was increased from 0.218 to 0.855 N in increments of 0.049 N, with strain sensitivities being  $-38.041$  and  $8.702$  pm/ $\mu\epsilon$  Linearities were  $R^2 = 0.99869$  and  $0.99495$ .

Xu et al. [39] utilised a thin core fibre (TCF) rather than PCF in the development of their sensor. By immersing the TCF in a Cargille Laboratories Inc. immersion oil and sealing the PCF within a capillary, the influences of external refractive indices was eliminated. The TCF was approximately 20 mm long with the protective capillary 40 mm long. A schematic of the sensor is given in **Figure 11**. Similar to PCF style temperature sensors, there was a resonant dip in the transmission spectrum, which was located at 1561.7 nm for the unfilled sensor. Temperature was modulated on an unspecified thermoelectric cooler, which could be controlled to 0.1 K resolution in the temperature range 288.15–318.15 K. Results were in good agreement with other published works, where a temperature sensitivity of 9.0 pm/K was recorded with a sensor linearity of  $R^2 = 0.9957$ .

The introduction of immersion oil (TOC =  $-3.95 \times 10^{-4}/K$ ) and capillary resulted in higher temperatures moving the resonance dip to a shorter wavelength, i.e. blue-shift, this being the converse of the bare TCF Mach-Zehnder Interferometer (TCFMI). Experimental results indicated that introduction of the immersion oil

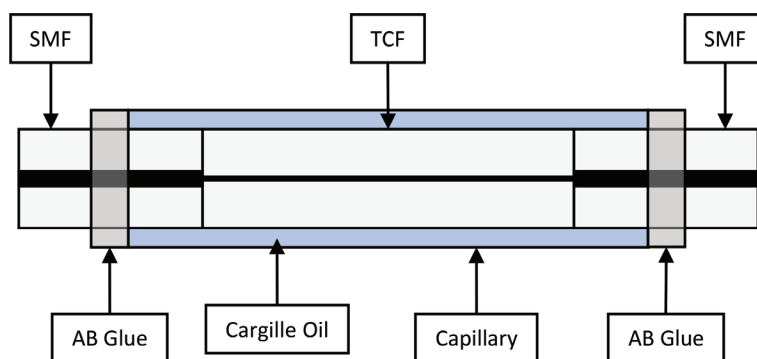


**Figure 11.**  
Schematic of sensor based on Xu et al. [39].

as a sealing fluid increased the temperature sensitivity of the interferometer  $>250\times$  compared to the baseline at  $-2.3$  nm/K. Heating and cooling the sensor showed repeatable results with the fitted polynomial having an  $R^2 = 0.999$ . It should be noted however at higher temperatures, the sensitivity decreased and the fitting error increased. Peak resolution was reported at 283.15 K as 0.008 K with an OSA resolution of 0.2 pm.

Xu et al. [39] went further to quantify the influence of strain on the sensor by measuring the temperature responses of a mechanically strained bare TCFMI, and an air-sealed TCFMI. Results indicated that the resonance-dip blue shifted with strain on the bare TCFMI, and the air sealed TCFMI appeared relatively temperature insensitive. The work concluded on the point of the sensitivity being primarily driven by the sealing fluid's thermo-optic coefficient. Again, however, the sensor required transmission of the light in order to be used, thus eliminating its potential to be used as a point sensor.

### 4.3 Sagnac interferometer type sensors

Qian et al. [44] presented an alcohol filled temperature sensor based on a highly birefringent photonic crystal fibre (HiBi-PCF) within a fibre loop mirror (FLM) as illustrated in **Figure 12**, the light source used was a super-luminescent light emitting diode (SLED). Owing to the birefringence of the HiBi-PCF, the counter-propagating waves caused by the 3 dB coupler have an optical path difference at recombination. Two resonant dips manifested in the transmission spectrum at 293.15 K, these being present at 1455.8 and 1549.8 nm. The sensor was tested in two conditions within an unspecified controlled temperature chamber. The first of these increasing from 293.15 to 307.15 K and the latter reducing the temperature from 293.15 to 281.15 K with the two resonant dips' responses being monitored. Measurement linearities were  $R^2 = 0.9995$  and  $R^2 = 0.9997$  respectively. Measured sensitivities were 6.2 and 6.6 nm/K compared to the theoretical values of 6.1 and 6.5 nm/K.

Cui et al. [45] proposed an SI type sensor similar in construction to that of Qian et al. [44]. The study conducted, however, went further in an effort to quantify the influence of selective hole filing in the PCF versus non-selective filling. Further to this, the length of PCF and hole fill ratio were explored. Simulations of no infiltration, all holes filled, small holes filled, and big holes filled were carried out; with the birefringence sensitivity to infiltrating liquid being monitored. While all three liquid filled cases indicated a reduced PCF birefringence, the 'big holes filled'

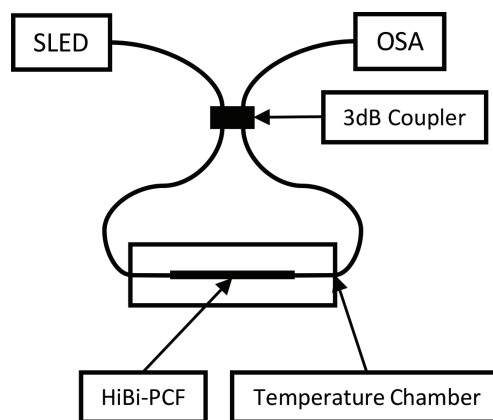


**Figure 12.**  
Schematic of HiBi-PCF sensor based on Qian et al. [44].

condition resulted in the highest temperature sensitivity, with a birefringence change of 27% as liquid refractive index was varied from 1.33 to 1.36. Dissimilar to the selective collapsing and cleaving method employed by Peng et al. [40] Cui et al. [45] offered a simplistic method of sealing the outer holes by introducing a micro-droplet of glue to the fibre face while monitoring with a microscope. It was claimed that the process could be conducted in under a minute with repeatable results after minimal training. During experimentation, water was used in place of ethanol due to the high coefficient of thermal expansion, and reduced tendency to evaporate. The sensor indicated a good sensitivity of  $-2.58$  nm/K with a linearity of  $R^2 = 0.9991$ . The OSA used to conduct the experiment had a resolution of  $0.02$  nm thus giving the sensor a resolution in the region of  $7.75$  mK. Accounting for the length of liquid filled PCF, results similar to that of Wang et al. [38] indicated increasing the ratio of filled to unfilled PCF increased temperature sensitivity.

#### **4.4 Similar sensors**

While one could consider liquid crystal based sensors in a similar category to those above, the authors wish to express they fall outside the remit of this chapter. However should the reader wish to explore these technologies, Windhorn and Cain [25] provides a good starting point. Several recent works exploring the use of liquid crystal thermometry using PCFs have also been published [53–55]. Wolinski et al. presented a multi-faceted liquid crystal PCF which was capable of temperature, electric field, and hydrostatic pressure detection [56].

### **5. Conclusions**

The remit of this review was to address current state-of-the-art LiF-OFTSs presented in literature. The optical fibre sensors examined were based on the principles of extrinsic Fabry-Perot interferometers, Mach-Zehnder interferometers and Sagnac interferometers. While sensitivities varied to an extent, they each presented performance equivalent to, or better than, reported electrical sensors. As noted in other reviews of optical fibre sensing such as that of Lee [57] and Poeggel et al. [58] optical fibre sensors had numerous additional advantages over their electronic counterparts such as immunity to EMI, small form factor, along with distributed and multiplexed sensing capability. Perhaps encouragingly, the commercial marketplace for optical fibre sensors appears to have matured significantly since the publication of Lee's review [57]. A driving factor in this will likely have been the coupled high resolution and fast response times, which are generally sub-Kelvin and sub-second respectively.

While FBGs remain the predominant method of temperature sensing, EFPI sensors have gained momentum in the commercial arena with companies such as FISO & Opsens offering varied ranges, sensitivities and sampling rates, indicating that they are slowly gaining favour in engineering and biomedical applications. That said however, MZI based temperature sensors were the more reported sensor type in literature. From this review it was obvious that while several ultra-high resolution liquid filled temperature sensors have been developed there is still scope for significant work to be carried out to improve their performance and stimulate widespread commercial deployment.

Considering that a significant portion of optical fibre sensor research has been focused towards biomedical applications in recent years, it is understandable that a market for inline sensors may not exist, that said however it may bode well for the

Company	Proximion	OPSENS	RJC Enterprises
Sensor name	WISTHEAT [60]	OTG-MPK5 [61]	N/A [62]
Sensor type	FBG	GaAs Crystal	EFPI
Min. temperature	228.15 K	293.15 K	288.15 K
Max. temperature	523.15 K	318.15 K	328.15 K
Resolution	70 mK(0.5 pm OSA)	10 mK	100 mK

**Table 2.**  
 Commercially available optical fibre temperature sensors.

designs of Chen et al. [46] and Poeggel et al. [34]. Another factor which has often been overlooked is the filling liquid properties, the majority of MZI sensors used an immersion oil provided by Cargille Laboratories Inc. and one reported using isopropanol. While the isopropanol may act as an irritant, the immersion oil used may be toxic if swallowed or inhaled, such as that of the Series AA [59]. It is also known to be damaging to waterways, thus indicating strict environmental controls require consideration. That said however, monitoring of industrial equipment using this method is more than plausible with the potential to use multiple PCFs on a single fibre to provide distributed sensing, **Table 2** lists example commercially available OFTSs. While the sensors are not of a liquid filled construction, they indicate the minimum required performance of any potential liquid filled sensor in order to potentially be commercially competitive.

## Conflict of interest

The authors wish to declare no conflict of interest.

## Nomenclature

Symbol	Name	Unit
D	Flexural rigidity	Pa.m <sup>3</sup>
E	Young's modulus	N/m <sup>2</sup>
P	Pressure	N/m <sup>2</sup>
Q	Heat	J
R	Outer radius	m
S <sub>T</sub>	Temperature sensitivity	/K
S <sub>ε</sub>	Strain sensitivity	-
T	Temperature	K
T <sub>0</sub>	Initial temperature	K
c	Specific heat capacity	J/kg.K
h	Thickness	m
n <sub>eff</sub>	Effective refractive index	-
r	Reference radius	m
t	Time	s
z	Deflection	m
Λ	Bragg grating pitch	m
α <sub>n</sub>	Thermal coefficient of refractive index	/K
α <sub>d</sub>	Thermal coefficient of thickness	/K
ε	Strain	-
λ	Wavelength	m
λ <sub>B</sub>	Bragg wavelength	m
ν	Poisson's ratio	-

## **Author details**

Fintan McGuinness<sup>1</sup>, Gabriel Leen<sup>1</sup>, Elfed Lewis<sup>1</sup>, Gerard Dooly<sup>2</sup>, Daniel Toal<sup>2</sup> and Dinesh Babu Duraibabu<sup>2\*</sup>


1 Optical Fibre Sensors Research Centre, University of Limerick, Limerick, Ireland

2 Centre for Robotics and Intelligent Systems, University of Limerick, Limerick, Ireland

\*Address all correspondence to: [dineshbabu.duraibabu@ul.ie](mailto:dineshbabu.duraibabu@ul.ie)

## **IntechOpen**

---

© 2018 The Author(s). Licensee IntechOpen. This chapter is distributed under the terms of the Creative Commons Attribution License (<http://creativecommons.org/licenses/by/3.0>), which permits unrestricted use, distribution, and reproduction in any medium, provided the original work is properly cited. 

## References

- [1] Valleriani M. Galileo Engineer. In: Cohen RS, Renn J, Gavroglu K, editors. *Boston Studies in the Philosophy of Science*. Vol. 269. Dordrecht: Springer Science + Business Media; 2010. pp. 155-165
- [2] McGee TD. *Principles and Methods of Temperature Measurement*. 1st ed. New York: Wiley-Interscience; 1988
- [3] Sverdrup H, Johnson MW, Fleming RH. *The Oceans, Their Physics, Chemistry, and General Biology*. New York: Prentice-Hall Inc.; 1942 [Internet]. Available from: <http://ark.cdlib.org/ark:/13030/kt167nb66r/>
- [4] Sarma U, Boruah PK. Design and development of a high precision thermocouple based smart industrial thermometer with on line linearization and data logging feature. *Measurement: Journal of the International Measurement Confederation*. 2010; **43**(10):1589-1594. DOI: 10.1016/j.measurement.2010.09.003 [Internet]
- [5] Yang F, Li G, Yang J, Wang Z, Han D, Zheng F, et al. Measurement of local temperature increments induced by cultured HepG2 cells with micro-thermocouples in a thermally stabilized system. *Scientific Reports*. 2017;**7**(1): 1-12. DOI: 10.1038/s41598-017-01891-1 [Internet]
- [6] Resistor Guide, NTC thermistor Resistor Guide [Internet]. Available from: <http://www.resistorguide.com/ntc-thermistor/> [Accessed: 25-07-2018]
- [7] Clow GD, Saltus RW, Waddington ED. A new high-precision borehole-temperature logging system used at GISP2, Greenland, and Taylor Dome, Antarctica. *Journal of Glaciology*. 1996; **42**(142):576-584. DOI: 10.3189/S0022143000003555 [Internet]. Available from: [https://www.cambridge.org/core/product/identifier/S0022143000003555/type/journal%7B%5C\\_%7Darticle](https://www.cambridge.org/core/product/identifier/S0022143000003555/type/journal%7B%5C_%7Darticle)
- [8] Hanna Instruments, Ultra-Fast Penetration K-Type Thermocouple Probe with Handle [Internet]. 2018. Available from: <https://hannainst.com/hi766c1-ultra-fast-penetration-%20k-type-thermocouple-probe-with-handle.html> [Accessed: 27-06-2018]
- [9] Hammond DL, Benjaminson A. The linear quartz thermometer—A new tool for measuring absolute and difference temperatures. *Hewlett-Packard Journal*. 1965;**16**(7):1-7 [Internet]. Available from: [ftp://dns.soest.hawaii.edu/bhowe/outgoing/20120920%7B%5C\\_%7DITU%7B%5C\\_%7DParis/HPJ-1965-03.pdf](ftp://dns.soest.hawaii.edu/bhowe/outgoing/20120920%7B%5C_%7DITU%7B%5C_%7DParis/HPJ-1965-03.pdf)
- [10] Lerch BA, Nathal MV. Thermocouple Calibration and Accuracy in a Materials Testing Laboratory. TM-2002-211507. Ohio: Glenn Research Centre, NASA; 2002
- [11] IEEE Standards Association. IEEE Std 2700<sup>TM</sup>-2014, IEEE Standard for Sensor Performance Parameter Definition. New York: IEEE; 2014. DOI: 10.1109/70 IEEESTD.2014.6880296
- [12] Rhoades R, Pflanzner R. In: Bachman C, editor. *Human Physiology*. 4th ed. Pacific Grove: Thomson Learning Inc.; 2003
- [13] Omega. TCC type correltaion. Tech. Rep. type C [Internet]. pp. 4-5. Available from: <https://www.omega.com/techref/pdf/z202.pdf>
- [14] Buckton G, Russell SJ, Beezer AE. Pharmaceutical calorimetry: A selective review. *Thermochimica Acta*. 1991;**193** (C):195-214. DOI: 10.1016/0040-6031(91)80184-K
- [15] Rossi S. Brain temperature, body core temperature, and intracranial

- pressure in acute cerebral damage. *Journal of Neurology, Neurosurgery & Psychiatry*. 2001;71(4):448-454. DOI: 10.1136/jnnp.71.4.448 [Internet]
- [16] NASA. Heat Transfer [Internet]. 2018. Available from: <https://wright.nasa.gov/airplane/heat.html> [Accessed: 12-07-2018]
- [17] Burgett RR, Massoll RE, Van Uum DR. Relationship between spark plugs and engine-radiated electromagnetic interference. *IEEE Transactions on Electromagnetic Compatibility*. 1974; **EMC-16**(3):160-172. DOI: 10.1109/TEMC.1974.303355
- [18] GE Oil & Gas. Platinum Resistance Thermometer (PRT) [Internet]. 2012. Available from: [https://geoilandgas.com/sites/geog/files/prt%7B%5C\\_%7Dplatinum%7B%5C\\_%7Dresistance%7B%5C\\_%7Dthermometer.pdf](https://geoilandgas.com/sites/geog/files/prt%7B%5C_%7Dplatinum%7B%5C_%7Dresistance%7B%5C_%7Dthermometer.pdf) [Accessed: 27-06-2018]
- [19] Hanna Instruments. K-Thermometers [Internet]. 2018. Available from: [https://hannainst.com/downloads/dl/file/id/1637/manhi%7B%5C\\_%7D93530%7B%5C\\_%7D531%7B%5C\\_%7D532.pdf](https://hannainst.com/downloads/dl/file/id/1637/manhi%7B%5C_%7D93530%7B%5C_%7D531%7B%5C_%7D532.pdf) [Accessed: 27-06-2018]
- [20] Shenzhen Senstech Electronic Technology Company Ltd. Waterproof Temperature Sensor DS18B20 Programmable Resolution 1-Wire Digital Thermometer [Internet]. 2018. Available from: [https://www.alibaba.com/product-detail/Waterproof-Temperature-Sensor-DS18B20-Programmable-%20Resolution%7B%5C\\_%7D1898805574.html?spm=a2700.7724857.main07.31.40cb3892YwvGzX](https://www.alibaba.com/product-detail/Waterproof-Temperature-Sensor-DS18B20-Programmable-%20Resolution%7B%5C_%7D1898805574.html?spm=a2700.7724857.main07.31.40cb3892YwvGzX) [Accessed: 27-06-2018]
- [21] Castellon J, Paez G, Strojnik M. Remote temperature sensor employing erbium-doped silica fiber. *Infrared Physics and Technology*. 2002;43(3-5): 219-222. DOI: 10.1016/S1350-4495(02)00142-1
- [22] Zhang H, Jiang Q, Wang BY, Wang JJ. Monitoring diesel engine parameters based on FBG probe. *Optoelectronics Letters*. 2016;12(5):0384-0388. DOI: 10.1007/s11801-016-6162-7
- [23] Pinet É, Hamel C, Glišić B, Inaudi D, Miron N. Health monitoring with optical fiber sensors: from human body to civil structures. In: Kundu T, editor. *SPIE Proceedings*. San Diego: SPIE; 19 May 2007;6532:653219-653230. DOI: 10.1117/12.715186. [Internet]. Available from: <http://proceedings.spiedigitallibrary.org/proceeding.aspx?articleid=1337730%20>; <http://proceedings.spiedigitallibrary.org/proceeding.aspx?doi=10.1117/12.715186>
- [24] Corning Incorporated. Frequently Asked Questions on Fiber Reliability [Internet]. 2016. Available from: <https://www.corning.com/media/worldwide/coc/documents/Fiber/RC-%20White%20Papers/WP5082%203-31-2016.pdf>
- [25] Windhorn TH, Cain CA. Optically active binary liquid crystal thermometry. *IEEE Transactions on Bio-Medical Engineering*. 1979;26(3): 148-152 [Internet]. Available from: <http://www.ncbi.nlm.nih.gov/pubmed/521025>
- [26] Poeggel S, Tosi D, Duraibabu D, Kelly J, Munroe M, Leen G, et al. Novel diaphragm microfabrication techniques for high-sensitivity biomedical fiber optic Fabry-Perot interferometric sensors. In: *Proceedings of SPIE—The International Society for Optical Engineering*. Vol. 9098. 2014. p. 909813. DOI: 10.1117/12.2050500 [Internet]. Available from: <http://proceedings.spiedigitallibrary.org/proceeding.aspx?doi=10.1117/12.2050500>
- [27] Nakazaki Y, Yamashita S. Fast and wide tuning range wavelength-swept fiber laser based on dispersion tuning and its application to dynamic FBG

- sensing. *Optics Express*. 2009;**17**(10): 8310. DOI: 10.1364/OE.17.008310 [Internet]. Available from: <https://www.osapublishing.org/abstract.cfm?URI=oe-17-10-8310>
- [28] Poeggel S, Duraibabu D, Tosi D, Leen G, Lewis E, McGrath D, et al. Differential *in vivo* urodynamic measurement in a single thin catheter based on two optical fiber pressure sensors. *Journal of Biomedical Optics*. 2015;**20**(3):037005. DOI: 10.1117/1.JBO.20.3.037005 [Internet]. Available from: <http://biomedicaloptics.spiedigitallibrary.org/article.aspx?doi=10.1117/1.JBO.20.3.037005>
- [29] Sellnau MC, Matekunas FA, Battiston PA, Chang C-F, Lancaster DR. Cylinder-Pressure-Based Engine Control Using Pressure-Ratio-Management and Low-Cost Non-Intrusive Cylinder Pressure Sensors no. 724 [Internet]. 2000. DOI: 10.4271/2000-01-0932. Available from: <http://papers.sae.org/2000-01-0932/>
- [30] Kasper JC, Wiggenhorn M, Resch M, Friess W. Implementation and evaluation of an optical fiber system as novel process monitoring tool during lyophilization. *European Journal of Pharmaceutics and Biopharmaceutics*. 2013;**83**(3):449-459. DOI: 10.1016/j.ejpb.2012.10.009 [Internet]
- [31] Hong CY, Zhang YF, Zhang MX, Leung LMG, Liu LQ. Application of FBG sensors for geotechnical health monitoring, a review of sensor design, implementation methods and packaging techniques. *Sensors and Actuators, A: Physical*. 2016;**244**:184-197. DOI: 10.1016/j.sna.2016.04.033 [Internet]
- [32] Gassino R, Pogliano J, Perrone G, Vallan A. Issues and characterization of fiber Bragg grating based temperature sensors in the presence of thermal gradients. *Measurement: Journal of the International Measurement Confederation*. 2018;**124**(January): 15-19. DOI: 10.1016/j.measurement.2018.03.049 [Internet]
- [33] Benham P, Crawford R, Armstrong C. *Mechanics of Engineering Materials*. 2nd ed. Harlow: Prentice-Hall Inc.; 1996
- [34] Poeggel S, Duraibabu D, Dooly G, Lewis E, Leen G. Novel ultrahigh resolution optical fibre temperature sensor. In: Lewis E, editor. *Proceedings of SPIE—The International Society for Optical Engineering*. Vol. 9916. 2016. p. 991605. DOI: 10.1117/12.2236155 [Internet]. Available from: <http://proceedings.spiedigitallibrary.org/proceeding.aspx?doi=10.1117/12.2236155>
- [35] Gao X, Yang M, Peng J, Lv D. Miniature fiber-optic temperature sensor based on optical coating interference. *Optik—International Journal for Light and Electron Optics*. 2017;**130**:1014-1020. DOI: 10.1016/j.ijleo.2016.11.114 [Internet]. Available from: <http://linkinghub.elsevier.com/retrieve/pii/S0030402616314516>
- [36] Hecht E. *Optics*. 5th ed. Harlow: Pearson Education Limited; 2014
- [37] Qiu S-j, Chen Y, Xu F, Lu Y-q. Temperature sensor based on an isopropanol-sealed photonic crystal fiber in-line interferometer with enhanced refractive index sensitivity. *Optics Letters*. 2012;**37**(5):863-865. DOI: 10.1364/OL.37.000863 [Internet]. Available from: <http://www.ncbi.nlm.nih.gov/pubmed/22378419>
- [38] Wang S, Liu Y-g, Wang Z, Han T, Xu W, Wang Y, et al. Intermodal interferometer based on a fluid-filled two-mode photonic crystal fiber for sensing applications. *Applied Optics*. 2013;**52**(14):3166-3171. DOI: 10.1364/AO.52.003166 [Internet]. Available from: <http://ao.osa.org/abstract.cfm?URI=ao-52-14-3166>
- [39] Xu B, Li J, Li Y, Xie J, Dong X. Liquid seal for temperature sensing with

- fiber-optic refractometers. *Sensors* (Switzerland). 2014;**14**(8):14873-14884. DOI: 10.3390/s140814873
- [40] Peng Y, Hou J, Zhang Y, Huang Z, Xiao R, Lu Q. Temperature sensing using the bandgap-like effect in a selectively liquid-filled photonic crystal fiber. *Optics Letters*. 2013;**38**(3): 263-265. DOI: 10.1364/OL.38.000263 [Internet]. Available from: <http://www.ncbi.nlm.nih.gov/pubmed/23381405>
- [41] Wang Y, Yang M, Wang DN, Liao CR. Selectively infiltrated photonic crystal fiber with ultrahigh temperature sensitivity. *IEEE Photonics Technology Letters*. 2011;**23**(20):1520-1522
- [42] Liang H, Zhang W, Geng P, Liu Y, Wang Z, Guo J, et al. Simultaneous measurement of temperature and force with high sensitivities based on filling different index liquids into photonic crystal fiber. *Optics Letters*. 2013;**38**(7): 1071-1073. DOI: 10.1364/OL.38.001071 [Internet]. Available from: <http://www.ncbi.nlm.nih.gov/pubmed/23546247>
- [43] Napolitano F. Fiber-Optic Gyroscopes Key Technological Advantages. Saint-Germain en Laye, Tech. Rep. [Internet]. 2010. Available from: <https://www.ixblue.com/m/publication/fog-key-advantages.pdf>
- [44] Qian W, Zhao C-L, He S, Dong X, Zhang S, Zhang Z, et al. High-sensitivity temperature sensor based on an alcohol-filled photonic crystal fiber loop mirror. *Optics Letters*. 2011;**36**(9):1548. DOI: 10.1364/OL.36.001548. arXiv: 0604155 [physics]. [Internet]. Available from: <https://www.osapublishing.org/abstract.cfm?URI=ol-36-9-1548>
- [45] Cui Y, Shum PP, Hu DJJ, Wang G, Humbert G, Dinh XQ. Temperature sensor by using selectively filled photonic crystal fiber Sagnac interferometer. *IEEE Photonics Journal*. 2012;**4**(5):1801-1808. DOI: 10.1109/JPHOT.2012.2217945
- [46] Qing Chen M, Zhao Y, Xia F, Peng Y, Jie Tong R. High sensitivity temperature sensor based on fiber air-microbubble Fabry-Perot interferometer with PDMS-filled hollow-core fiber. *Sensors and Actuators, A: Physical*. 2018;**275**:60-66. DOI: 10.1016/j.sna.2018.03.044 [Internet]
- [47] Poeggel S, Duraibabu D, Kalli K, Leen G, Dooly G, Lewis E. Recent improvement of medical optical fibre pressure and temperature sensors. *Biosensors*. 2015;**5**(3):432-449. DOI: 10.3390/bios5030432 [Internet]. Available from: <http://www.mdpi.com/2079-6374/5/3/432/>
- [48] Sensortec B. Data sheet. Tech. Rep. [Internet]. 2009. Available from: <https://www.sparkfun.com/datasheets/Components/General/BST-BMP085-DS000-05.pdf>
- [49] NKT Photonics. LMA-8. Tech. Rep. [Internet]. Available from: <https://www.nktpotonics.com/wp-content/uploads/sites/3/2015/01/LMA-8.pdf>
- [50] Jha R, Villatoro J, Badenes G, Pruneri V. Refractometry based on a photonic crystal fiber interferometer. *Optics Letters*. 2009;**34**(5):617. DOI: 10.1364/OL.34.000617 [Internet]. Available from: <https://www.osapublishing.org/abstract.cfm?URI=ol-34-5-617>
- [51] Qiu S-j, Chen Y, Kou J-l, Xu F, Lu Y-q. Miniature tapered photonic crystal fiber interferometer with enhanced sensitivity by acid microdroplets etching. *Applied Optics*. 2011;**50**(22):4328. DOI: 10.1364/AO.50.004328 [Internet]. Available from: <https://www.osapublishing.org/abstract.cfm?URI=ao-50-22-4328>
- [52] Gong H, Chan CC, Zhang YF, Wong WC, Dong X. Miniature refractometer based on modal interference in a hollow-core photonic crystal fiber with

- collapsed splicing. *Journal of Biomedical Optics*. 2011;**16**(1):017004. DOI: 10.1117/1.3527259 [Internet]. Available from: <http://biomedicaloptics.spiedigitallibrary.org/article.aspx?doi=10.1117/1.3527259>
- [53] Wolinski TR, Szaniawska K, Ertman S, Lesiak P, Domanski AW, Dabrowski R, et al. Influence of temperature and electrical fields on propagation properties of photonic liquid-crystal fibres. *Measurement Science and Technology*. 2006;**17**(5):985-991. DOI: 10.1088/0957-0233/17/5/S08 [Internet]. Available from: <http://stacks.iop.org/0957-0233/17/i=5/a=S08?key=crossref.f9489a53384ab98a6cd800efb7324542>
- [54] Wei L, Eskildsen L, Weirich J, Scolari L, Alkeskjold TT, Bjarklev A. Continuously tunable all-in-fiber devices based on thermal and electrical control of negative dielectric anisotropy liquid crystal photonic bandgap fibers. *Applied Optics*. 2009;**48**(3):497. DOI: 10.1364/AO.48.000497 [Internet]. Available from: <https://www.osapublishing.org/abstract.cfm?URI=ao-48-3-497>
- [55] Miao Y, Liu B, Zhang K, Liu Y, Zhang H. Temperature tunability of photonic crystal fiber filled with Fe<sub>3</sub>O<sub>4</sub> nanoparticle fluid. *Applied Physics Letters*. 2011;**98**(2):21103. DOI: 10.1063/1.3540647
- [56] Wolinski T, Czapl A. Photonic liquid crystal fibers for sensing applications. *IEEE Transactions on Instrumentation and Measurement*. 2008;**57**(8):1796-1802. DOI: 10.1109/TIM.2008.922077 [Internet]. Available from: [http://ieeexplore.ieee.org/xpls/abs%7B%5C\\_%7Dall.jsp?arnumber=4510764](http://ieeexplore.ieee.org/xpls/abs%7B%5C_%7Dall.jsp?arnumber=4510764)
- [57] Lee B. Review of the present status of optical fiber sensors. *Optical Fiber Technology*. 2003;**9**(2):57-79. DOI: 10.1016/S1068-5200(02)00527-8
- [58] Poeggel S, Tosi D, Duraibabu D, Leen G, McGrath D, Lewis E. Optical fibre pressure sensors in medical applications. *Sensors*. 2015;**15**(7):17115-17148. DOI: 10.3390/s150717115 [Internet]. Available from: <http://www.mdpi.com/1424-8220/15/7/17115/>
- [59] Cargille Laboratories Inc. Cargille Refractive Index Liquid Series AA nD = 1.400–1.459 Safety Data Sheet [Internet]. Available from: [http://www.cargille.com/SDS%7B%5C\\_%7DRI%7B%5C\\_%7DSeries%7B%5C\\_%7DAA.pdf](http://www.cargille.com/SDS%7B%5C_%7DRI%7B%5C_%7DSeries%7B%5C_%7DAA.pdf)
- [60] Proximion. High Temperature FBG Sensor for Harsh Environment [Internet]. Available from: [https://static1.squarespace.com/static/54690ca0e4b0dc0a73f1772b/t/57f752ed579fb360231dc1f4/1475826414976/Proximion%7B%5C\\_%7Dprodblad%7B%5C\\_%7DWISTHEAT%7B%5C\\_%7D161005.pdf](https://static1.squarespace.com/static/54690ca0e4b0dc0a73f1772b/t/57f752ed579fb360231dc1f4/1475826414976/Proximion%7B%5C_%7Dprodblad%7B%5C_%7DWISTHEAT%7B%5C_%7D161005.pdf) [Accessed: 12-07-2018]
- [61] OpSens. OTG-MPK5 Fiber Optic Temperature Sensor, Probe and Transducer [Internet]. 2018. Available from: <https://opsens-solutions.com/products/fiber-optic-temperature-sensors/otg-mpk5/> [Accessed: 12-07-2018]
- [62] RJC Enterprises. How Our Sensors Work [Internet] 2018. Available from: <http://www.rjcenterprises.net/background.html> [Accessed: 12-07-2018]